

Image-to-Text for Medical Reports Using Adaptive Co-Attention and Triple-LSTM Module

Yishen Liu, Shengda Luo, Zishao Zhong, Hudan Pan[†]

Chinese Medicine Guangdong Laboratory

E-mail: liuyishen0226@163.com

Abstract—Medical report generation requires specialized expertise that general large models often fail to accurately capture. Moreover, the inherent repetition and similarity in medical data make it difficult for models to extract meaningful features, resulting in a tendency to overfit. So in this paper, we propose a multimodal model, Co-Attention Triple-LSTM Network (CA-TriNet), a deep learning model that combines transformer architectures with a Multi-LSTM network. Its Co-Attention module synergistically links a vision transformer with a text transformer to better differentiate medical images with similarities, augmented by an adaptive weight operator to catch and amplify image labels with minor similarities. Furthermore, its Triple-LSTM module refines generated sentences using targeted image objects. Extensive evaluations over three public datasets have demonstrated that CA-TriNet outperforms state-of-the-art models in terms of comprehensive ability, even pre-trained large language models on some metrics.

Index Terms—image captioning, co-attention mechanism, medical report generation, LSTM, multi-label classification

I. INTRODUCTION

Large Language Models (LLMs) have demonstrated remarkable success in generating medical reports [1], like GPT [2] and Med-Gemini [3], offering advantages in enhancing efficiency and consistency. Fine-tuning techniques, such as LoRA [4], combined with training on specific datasets, enable large models to perform more specialized tasks with improved precision and adaptability [5], like niche areas, such as Traditional Chinese Medicine (TCM) LLMs [6], [7]. However, they face challenges in accuracy, contextual understanding and interpretability [8]. Moreover, the hardware requirements and computational power needed to train LLMs present significant challenges, limiting accessibility and scalability.

Unlike LLMs for medical report generation, there are also many small but exquisite models, based on Encoder-Decoder framework [9]–[14]. Moreover, they further enhanced this approach by introducing attention mechanisms [15], [16]. For the encoder part, vision transformer like ViT [16] is added on convolutional neural networks (CNN) or other computer vision (CV) models, which decomposes an input image into a series of patches and serializes each patch into a vector, and maps it to a smaller dimension with a single matrix multiplication. For the decoder part, transformer-based natural language processing (NLP) techniques [15] tokenize and process text,

ensuring that the generated descriptions are more coherent and contextually relevant. Small models of this type excel in specialized tasks, sometimes surpassing larger models in specific domains, though they remain limited in versatility [1]. However, literatures [17], [18] demonstrate that when CNN parameters are optimized and training strategies are adapted to the data’s underlying characteristics, CNNs can achieve performance superior to transformers. So does transformers [15], [16].

Additionally, current datasets exhibit specific deficiencies [19], such as similarity in medical imaging, redundancy in data labeling, and erroneous multi-label classification. What is more, small dataset like IU X-ray and PEIR Gross [11], [20] are not suitable for the vision transformer [16], because it can provide advanced image feature extraction but demand extensive pre-training, often causing fitting problems [21].

To tackle these challenges, we proposes the Co-Attention Triple-LSTM Network (CA-TriNet) for efficient and high-quality medical report generation. CA-TriNet employs an Encoder-Decoder framework with two components: a Co-Attention module (encoder) that combines transformers to differentiate similar medical images and optimize feature transfer using adaptive weights, and a Triple-LSTM module (decoder) that refines sentence generation by focusing on targeted image objects.

All in all, we make the following contributions:

- We present a multimodal model, CA-TriNet that consists of Co-Attention mechanism and Triple-LSTM module, which enhances image feature extraction, improves text relevance, and tackles imprecise label classification for the first time.
- We propose an adaptive weight similarity operator that improves training by dynamically adjusting multi-head attention for better learning and enhancing efficiency by mitigating redundant data labeling, thereby aligning image features with their labels effectively.
- Experimental results on three public medical datasets demonstrate that the CA-TriNet model surpasses state-of-the-art performance in terms of comprehensive ability, even comparable to LLMs in some indicators.

[†] Corresponding Author

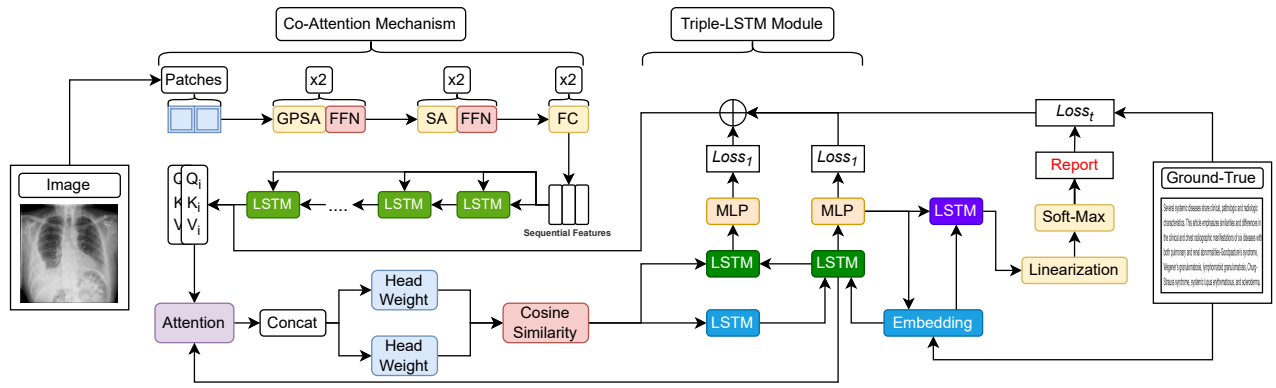


Fig. 1. CA-TriNet comprises two major components: the Co-Attention Mechanism and the Triple-LSTM Module, including a multi-label classification part.

II. RELATED WORK

A. Image Captioning

Image captioning generates descriptive sentences for images and has advanced significantly over the past decade [9]. Early models used CNNs with RNNs or LSTMs [22]–[25], while later works introduced visual attention [22], [23]. Recent transformer-based architectures [26], [27] enhance global context modeling and vision-language alignment, providing foundational concepts for tasks like medical report generation.

B. Medical Report Generation

Medical report generation extends image captioning by producing accurate, context-rich reports for medical images, requiring domain expertise to detect subtle symptoms [20]. Early CNN-RNN frameworks [11], [22], [28] evolved into transformer-based models [29]–[33], improving clinical accuracy through multimodal integration. Challenges persist in detecting subtle pathologies and interpreting clinical terminology accurately. Recently, LLMs [2], [6], [34], [35] are used for report generation or summary. They employ fine-tuning techniques [1], [4] to enhance accuracy on specialized tasks. However, the high training costs and challenges of data development often deter small laboratories from adopting it. Additionally, for smaller tasks or niche applications, LLMs can appear overly complex and redundant. In such cases, the importance of small, precise AI models becomes evident [3], [33].

So, we propose CA-TriNet, a model combining a co-attention mechanism with Triple-LSTM architecture to improve image feature extraction and text alignment, which is tailored for medical report generation. An adaptive weight similarity operator enhances multi-head attention, boosting training efficiency and reducing label redundancy. Evaluations show CA-TriNet outperforms state-of-the-art methods and matches large language models on some metrics.

III. METHODOLOGY

Fig. 1 has shown the structure of CA-TriNet and we provide a detailed explanation of the two modules and the associated loss function in the next section.

A. Co-Attention Mechanism

First, the Co-Attention module serves as the encoder, combining ConViT [36] and transformer [15] features via fully connected layers (FC) and a self-parallel LSTM, an image feature extraction (IFE) component [21], [37]. A multi-head attention mechanism with double-head weights and a cosine similarity operator adaptively adjusts weights to enhance key feature extraction.

ConViT processes pathological images with SA (SA = self-attention), GPSA (GPSA = gated positional self-attention), and FFN (FFN = feedforward network) layers to generate embedding features ($F_{embedding}$), refined into one-dimensional vectors via FC. An LSTM then produces bag-of-words features (F_{CL}), integrating local and global image data to improve language prediction accuracy.

The multi-head attention mechanism computes multiple independent attentions using matrices Q , K , and V . Each head, linearly transformed, focuses on a specific output subspace, with N heads dividing the sequence into $\frac{1}{N}$ parts. After training, task-relevant heads receive higher weights. To exploit these, we introduce a secondary weighting mechanism that selects the head with the highest weight (w_a) at each step. As demonstrated on the IU X-ray dataset (Fig. 2), this approach enhances performance by prioritizing critical features. On this basis, we introduce cosine weight ($\cos(i)^j$) to represent the cosine similarity between head j and base at i iteration, as shown in Eq. 1.

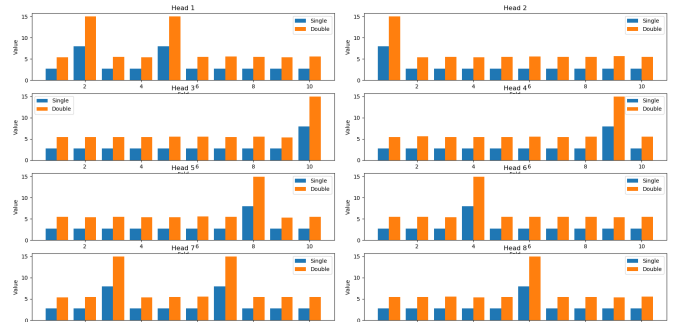


Fig. 2. Comparison of single and double weights for IU X-ray ($N=8$) shows the secondary weighting mechanism enhances key attention heads, which gain higher weights after training, while others play minor roles.

$$\cos(i)^j = \cos(\text{head}_{att(i-1)}^j, \text{head}_{att(i-1)}^{base}) \quad (1)$$

where $\cos(i)^j \notin [-1, 1]$, $\text{head}_{att(i-1)}^j$ is the weight of the j -th header processed by the attention mechanism.

For each batch, the cosine similarity of the same head will sum up and divide by the number of heads to compute the second weight $W_{cos(i)}^j$, as shown in Eq. 2.

$$w_{cos(i)}^j = \frac{\sum_{k \in i} \cos(i)_k^j}{N} \quad (2)$$

Where $\cos(i)_k^j$ is the cosine similarity between head j and base of data k and N is the number of heads. The concatenation of $w_{cos(i)}^j$ ($j = 1, 2, \dots, N$) is the second weight $w_{cos(i)}$. The final attention output is calculated by both weights, as shown in Eq. 3.

$$w_{cos(i)} = \text{Concat}(w_{cos(i)}^1, \dots, w_{cos(i)}^j) \quad (3)$$

After this step, we designed a new weight balancing function, Eq. 4.

$$w_{dwa(i)}^j = \lambda - w_{cos(i)} \quad (4)$$

To address this, we introduce λ and design a weight function $w_{dwa(i)}^j$ to improve the model's focus on pathological regions. When normal samples are highly similar, the second weight increases. This approach helps the model prioritize key information while processing general data efficiently, saving computational resources.

TABLE I
FEATURE CONFIDENCE INTERVAL OF THE IU X-RAY DATASET.

HEAD	MEAN	SD	CI (0.95)
1	0.7500	0.2812	0.1949
2	-0.0240	0.0078	0.0054
3	0.0893	0.0208	0.0144
4	0.0686	0.0201	0.0140
5	0.0338	0.0103	0.0071
6	-0.0484	0.0133	0.0092
7	-0.0030	0.0155	0.0108
8	-0.0516	0.0236	0.0164

We also calculated the 95% confidence interval (CI) and Standard Deviation (SD) for each head based on cosine similarity and the distribution of cosine weights (Tab. I). Cosine similarity and weight distribution for the IU X-ray dataset were analyzed over 25,673 iterations in a single training epoch. For values above 0, most correspond to normal datasets, with similar label descriptions. Disease data, with varied descriptions, often result in negative values. To emphasize these negative samples, we set λ as the harmonic mean (Eq. 5):

$$\lambda = \frac{n}{\sum_1^n (w_{cos(i)})^{-1}} \quad (5)$$

This strengthens negative sample weights. As shown in Tab. I, λ increases when deviating from a negative weight and

decreases when deviating from a positive weight. It prioritizes low-order data, with negative values set to 0 by the RELU function, making subsequent calculations simpler. The model focuses on learning from negative samples while minimizing attention to positive ones.

B. Triple-LSTM Module

Medical image datasets, annotated with disease labels, are crucial for multi-label classification models but face challenges due to limited dataset size relative to label variety [10], [22]. To address this, we propose a Triple-LSTM structure, treating labels as a 'quality enhancement module' (Fig. 1). CA-TriNet consists of three LSTMs. LSTM (blue) is just used to encode features from Dual-Attention Mechanism, as expressed in Eq. 6.

$$h_t^1 = \text{LSTM}(T_t^1, w_{dwa(i)}^j * \text{att}_{a(i)}^j) \quad (6)$$

where T_t^1 denotes the word embedding of transformer generated. When the first LSTM (dark green) decode the first time, the inputs are T_t^1 , h_t^1 , the word embedding $W_e^2 x_t$ and the hidden state of LSTM, h_{t-1}^2 , as shown in Eq. 7.

$$h_t^2 = \text{LSTM}(T_t^1, h_t^1, W_e^2 x_t, h_{t-1}^2) \quad (7)$$

Then the probability of next word can be predicted by a MLP, as appeared in Eq. 8:

$$\text{MLP}_{t+1}^1 = \text{softmax}(W_{FC1} * h_t^2) \quad (8)$$

Where W_{FC1} is the fully connected layer of MLP. So does the second LSTM (dark green), as shown in Eq. 10.

$$h_t^3 = \text{LSTM}(T_t^2, h_t^2, W_e^2 x_t) \quad (9)$$

$$\text{MLP}_{t+1}^1 = \text{softmax}(W_{FC2} * h_t^3) \quad (10)$$

After that, the text features generated by the two MLPs are used to calculate the loss functions and use it in the later stage.

The model incorporates a multi-label classification module (LSTM-Purple) that uses generated sentences as input instead of images. LSTM-Purple processes embedded report representations (RP_{emb}) to predict categories, enhancing report quality. is fed into LSTM-Purple, producing preliminary category predictions ($Label$) based on the report's semantic content and context, as shown in Eq. 11.

$$Label = \text{softmax}(W_t \cdot \text{LSTM}(RP_{emb}) + b_t) \quad (11)$$

where W_t and b_t are trainable parameters used to flatten $\text{LSTM}(RP_{emb})$.

Subsequently, $Label$ is linearly transformed via a mapping layer and processed with a softmax function to produce a probability distribution over potential labels. This module enhances report accuracy by aligning generated content with diagnostic labels, refining medical image-based report generation.

C. Loss Function

For the loss functions, we use $loss_1$ and $loss_2$ which are the cross-entropy loss between reports generated by the first (second) LSTM-2 in the H-Decoder and true captions, respectively. The second LSTM-2 generation is confined by an adjustable parameter $\alpha \in (0, 1]$. Coefficient $\beta, \in (1, 10]$, starting at 5, is designed to balance $loss_1$, $loss_2$ and $loss_t$. For $loss_t^1$, it is shown in Eq. 12.

$$loss_t = -\frac{1}{C} * \sum Tag_i * \log(sig(tag)) + (1 - Tag_i) * \log(sig(tag))^{-1} \quad (12)$$

where Tag represents the true tags, $i \in \{0, 1, \dots, n - 1\}$, $Tag_i \in \{0, 1\}$, n is the number of tags types. As a result, the model $loss$ is calculated as the follow Eq. 13:

$$loss = loss_t + \alpha * loss_1 + \beta * loss_2 \quad (13)$$

IV. DATASETS AND IMPLEMENT

A. Dataset

The datasets utilized include **IU X-Ray**² [20], comprising 7,470 chest X-ray image-report pairs curated for automated captioning and X-ray interpretation; **PEIR Gross**³ [11], containing 7,442 image-caption pairs across 21 categories, supporting medical education and image captioning; **Mimic Chest X-Ray**⁴ [38], a large-scale dataset of 371,920 radiographs from 227,943 studies for machine learning in diagnostic imaging. For dataset pre-processing, refer to survey [20].

B. Implement

1) *Evaluation Matrix*: we choose three widely-used metrics to evaluate our work: BLEU [39], ROUGE-L [40], and CIDER [41]. These metrics were originally developed for distinct purposes: BLEU for machine translation evaluation, ROUGE-L for summarization quality assessment, and CIDER for image caption evaluation. Each metric emphasizes different aspects such as fluency, accuracy, and human-likeness. Nonetheless, in all cases, higher scores indicate better performance. Finally, we use B-1 (BLEU-1), B-2 (BLEU-1), B-3 (BLEU-1), B-4 (BLEU-1), Rou (ROUGEL) and CID (Cider) to represent these indicators.

2) *Hyperparameter*: we utilize ConViT [36] pretrained on ImageNet [42], excluding the final classification layer, to extract 512-dimensional visual features. Both the word embedding dimension and the hidden state dimension of all LSTMs are also set to 512. We adopt ADAM [43] as the optimizer throughout our model. The learning rate is 0.0004. Beam search is utilized during evaluation, with metrics calculated via a widely used image captioning framework.

¹MultiLabel- SoftMarginLoss: <https://pytorch.org/docs>

²<https://openi.nlm.nih.gov>

³<https://peir.path.uab.edu/library/>

⁴<https://physionet.org/content/mimic-cxr/>

TABLE II

COMPARISON OF CA-TRI-NET WITH STATE-OF-THE-ART FRAMEWORKS AND PRE-TRAINED LATEST LLMs ON THREE DATASETS. RED MEANS THAT INDICATORS SURPASS THE EFFECTS OF CA-TRI-NET. (×100%)

MODEL	DATASET	B-1	B-2	B-3	B-4	Rou	CID
CNN-RNN [22]	IU X-RAY	38.1	29.0	22.7	16.0	39.6	31.2
CO-ATT [11]		46.2	33.1	24.2	17.8	40.5	40.8
JE-Tri [31]		47.8	34.4	24.8	18.0	39.8	43.9
TRANSGEN [33]		46.1	28.5	19.6	14.5	36.7	35.1
M2TRANS [32]		46.3	31.8	21.4	15.5	33.5	34.9
PPKED [44]		48.3	31.5	22.4	16.8	37.7	44.9
ARRG [45]		49.6	31.9	24.1	17.5	37.6	35.1
AENSI [10]		52.1	35.9	26.1	20.8	42.2	43.2
CA-TriNET (Ours)		54.6	38.7	28.4	21.3	44.1	47.2
BOOTSTRAPPINGLLM [46]		49.9	32.3	23.8	18.4	39.0	-
R2GENGPT [34]	46.5	29.9	21.4	16.1	40.1	54.2	
R2GENCSR-LLAMA2 [35]	51.4	35.1	26.2	20.6	40.1	57.9	
CO-ATT [11]	PEIR GROSS	30.0	21.8	16.5	11.3	27.9	32.9
M2TRANS [32]		45.1	30.7	20.6	14.3	32.1	33.2
SVEH [21]		46.6	32.3	23.3	16.9	37.4	26.9
AENSI [10]		44.2	31.5	22.6	17.4	38.5	28.2
PPKED [44]		43.1	30.2	20.9	16.8	39.7	34.3
CA-TriNET (Ours)		51.2	36.3	27.6	21.1	44.9	37.2
CNN-RNN [22]	CHEST X-RAY	29.9	18.4	12.1	8.4	26.3	11.2
M2TRANS [32]		21.2	12.8	8.3	5.8	24.0	7.4
ARRG [45]		35.1	22.3	15.7	11.8	28.7	28.1
AENSI [10]		34.0	21.1	14.3	12.1	29.7	25.2
CA-TriNET (Ours)		40.8	25.8	17.9	14.1	31.2	29.8
BOOTSTRAPPINGLLM [46]		40.2	26.2	18.0	12.8	29.1	-
R2GENGPT [34]		40.8	25.6	17.4	12.5	28.5	24.4
R2GENCSR-LLAMA2 [35]		42.0	26.8	18.6	13.6	29.1	26.7

V. EXPERIMENTAL RESULTS

We conducted experiments (Tab. II) comparing our model with state-of-the-art approaches, demonstrating superior performance on smaller datasets like IU X-ray and PEIR Gross, attributed to its architecture and innovative feature distribution mechanism. On the larger Mimic Chest X-ray dataset, its diverse and uniform samples enhanced model generalizability, with modest performance gains translating to significant clinical improvements. For LLMs, on the small-sample IU X-Ray dataset, LLMs achieve higher CIDER scores. This is because small models, constrained by limited corpora with high annotation repetition rates, generate more formulaic reports, while large models leverage extensive pre-trained corpora to produce more polished outputs. Large datasets offer richer corpora, mitigating this issue. Instead, differences appear in sentence length (BLEU), with LLMs favoring concise, precise summaries.

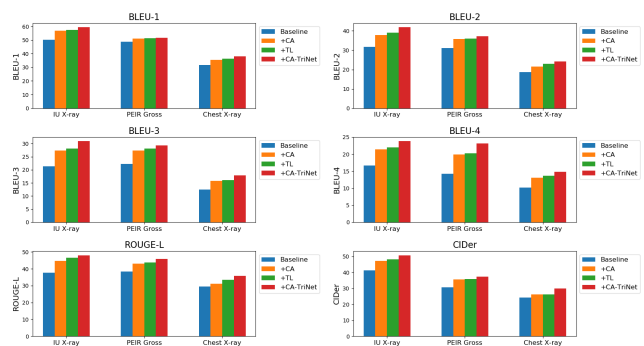


Fig. 3. Ablation experiment of our model On IU X-ray, PEIR Gross and Chest X-ray datasets. (CA = Co-Attention Mechanism, TL = Triple-LSTM Module)

As shown in Fig. 3, we performed ablation experiments on the IU X-ray, PEIR Gross, and Chest X-ray datasets to assess the contributions of each proposed component. The

baseline model consists of ViT [16], the transformer [15], LSTM [21]. The results demonstrate clear performance gains with the inclusion of our modules, with the comprehensive CA-TriNet model achieving the best overall results.

TABLE III
COMPARISON OF MODELS WITH THEIR IMPROVED VERSIONS (WITH ADAPTIVE WEIGHT SIMILARITY OPERATOR) ON FOUR PUBLIC DATASETS. (BLUE MEANS MODELS' PLUS VERSIONS) ($\times 100\%$)

Model	Dataset	B-1	B-2	B-3	B-4	Rou	CID
JE-Tri [31]	IU X-ray	47.8	34.4	24.8	18.0	39.8	43.9
JE-Tri		48.5	35.0	25.5	18.5	40.5	44.5
TransGen [33]		46.1	28.5	19.6	14.5	36.7	35.1
TransGen		46.8	29.0	20.2	15.0	37.5	35.8
M2Trans [32]		46.3	31.8	21.4	15.5	33.5	34.9
M2Trans		47.0	32.5	22.0	16.0	34.2	35.5
M2Trans [32]	PEIR Gross	45.1	30.7	20.6	14.3	32.1	33.2
M2Trans		45.8	31.3	21.2	14.8	32.8	33.8
SVEH [21]		46.6	32.3	23.3	16.9	37.4	26.9
SVEH		47.2	32.9	23.9	17.5	38.0	27.5
PPKED [44]		43.1	30.2	20.9	16.8	39.7	34.3
PPKED		43.8	30.8	21.5	17.4	40.5	34.9
M2Trans [32]	Chest X-ray	21.2	12.8	8.3	5.8	24.0	7.4
M2Trans		21.8	13.3	8.8	6.2	24.5	7.8
ARRG [45]		35.1	22.3	15.7	11.8	28.7	28.1
ARRG		35.8	22.9	16.3	12.3	29.5	28.8
ARRG							

Tab. III shows that our adaptive weight similarity operator significantly improves performance, especially on smaller datasets with more negative samples. The smaller gains on larger datasets suggest that statistical data properties affect performance, aligning with findings in related studies [17], [18]. Finally, we visualize our results, as appeared in Fig. 4. Compared with Ground-True, reports generated by CA-TriNet are simpler and easier to understand, without too many long and difficult sentences. This facilitates quick reading and comprehension.

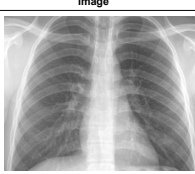
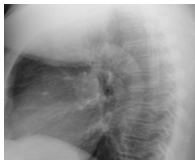
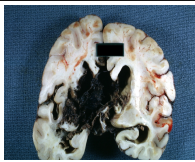
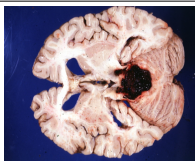
Image	Ground-True	Our Model
	No acute cardiopulmonary abnormality. Heart size and mediastinal contours appear within normal limits. Pulmonary vascularity is within normal limits. No focal consolidation, suspicious pulmonary opacity, pneumothorax or definite pleural effusion. Visualized osseous structures appear intact.	No acute cardiopulmonary abnormality. Lungs are clear bilaterally. No focal consolidation, pleural effusion, or pneumothoraces. Cardiomeastinal silhouette appears normal. Heart size appears normal. Osseous structures is intact.
	No acute cardiopulmonary abnormality. Mediastinal contours are normal. Lungs are clear. There is no pneumothorax or large pleural effusion.	No acute cardiopulmonary abnormality. Lungs are clear. No focal consolidation, pleural effusion, or pneumothoraces.
	GROSS: NERVOUS: Brain: Hemorrhage: Gross large hemorrhagic infarct basal ganglia rupture into ventricle.	GROSS: NERVOUS: Brain: Hemorrhage: large size hemorrhagic infarct, basal ganglia with rupture into the ventricle.
	GROSS: NERVOUS: Pons: Hemorrhage: Gross fixed tissue but good color massive pontine hemorrhage not due to pressure do not have history at this time good photo.	GROSS: NERVOUS: Pons: Hemorrhage: Gross fixed tissue good pontine hemorrhage, not from pressure. No history available at this moment. Good photo.

Fig. 4. Experimental results of report generated by CA-TriNet.

VI. CONCLUSION

In this paper, we propose CA-TriNet, a model for medical report generation that combines a Co-Attention Mechanism for extracting image features with a Triple-LSTM Module for integrating previous sentences during report generation. An adaptive weight similarity operator, based on the geometric mean, is designed to amplify features of negative (diseased) samples and selectively downweight positive samples, improving performance on small, feature-imbalanced datasets like IU X-ray, PEIR Gross, as well as large-scale dataset, Mimic Chest X-ray. The results demonstrate that understanding dataset-specific patterns and optimizing feature transfer yields better outcomes than simply stacking models.

REFERENCES

- [1] Hongjian Zhou, Fenglin Liu, Boyang Gu, Xinyu Zou, Jinfa Huang, Jinge Wu, Yiru Li, Sam S Chen, Peilin Zhou, Junling Liu, et al., "A survey of large language models in medicine: Progress, application, and challenge," *arXiv preprint arXiv:2311.05112*, 2023.
- [2] Josh Achiam, Steven Adler, Sandhini Agarwal, Lama Ahmad, Ilge Akkaya, Florencia Leoni Aleman, Diogo Almeida, Janko Altmenschmidt, Sam Altman, Shyamal Anadkat, et al., "Gpt-4 technical report," *arXiv preprint arXiv:2303.08774*, 2023.
- [3] Khaled Saab, Tao Tu, Wei-Hung Weng, Ryutarō Tanno, David Stutz, Ellery Wulczyn, Fan Zhang, Tim Strother, Chungjong Park, Elahe Vedadi, et al., "Capabilities of gemini models in medicine," *arXiv preprint arXiv:2404.18416*, 2024.
- [4] Edward J Hu, Yelong Shen, Phillip Wallis, Zeyuan Allen-Zhu, Yuanzhi Li, Shean Wang, Lu Wang, and Weizhu Chen, "Lora: Low-rank adaptation of large language models," *arXiv preprint arXiv:2106.09685*, 2021.
- [5] Haotian Liu, Chunyuan Li, Qingyang Wu, and Yong Jae Lee, "Visual instruction tuning," *Advances in neural information processing systems (NIPS)*, vol. 36, 2024.
- [6] Hongbo Zhang, Junying Chen, Feng Jiang, Fei Yu, Zhihong Chen, Guiming Chen, Jianquan Li, Xiangbo Wu, Zhang Zhiyi, Qingying Xiao, Xiang Wan, Benyou Wang, and Haizhou Li, "HuatuoGPT, towards taming language model to be a doctor," in *Findings of the Association for Computational Linguistics: EMNLP 2023*, Singapore, Dec. 2023, pp. 10859–10885, Association for Computational Linguistics.
- [7] Yudong Li, Yuhao Feng, Wen Zhou, Zhe Zhao, Linlin Shen, Cheng Hou, and Xianxu Hou, "Dynamic data sampler for cross-language transfer learning in large language models," in *ICASSP 2024-2024 IEEE International Conference on Acoustics, Speech and Signal Processing (ICASSP)*. IEEE, 2024, pp. 11291–11295.
- [8] Mark Chen, Jerry Tworek, Heewoo Jun, Qiming Yuan, Henrique Ponde De Oliveira Pinto, Jared Kaplan, Harri Edwards, Yuri Burda, Nicholas Joseph, Greg Brockman, et al., "Evaluating large language models trained on code," *arXiv preprint arXiv:2107.03374*, 2021.
- [9] Guangyi Liu, Yinghong Liao, Fuyu Wang, Bin Zhang, Lu Zhang, Xiaodan Liang, Xiang Wan, Shaolin Li, Zhen Li, Shuixing Zhang, and Shuguang Cui, "Medical-vlbnet: Medical visual language bert for covid-19 ct report generation with alternate learning," *IEEE Transactions on Neural Networks and Learning Systems*, vol. 32, no. 9, pp. 3786–3797, 2021.
- [10] Yihan Lin, Qian Tang, Hao Wang, Cheng Huang, Ekong Favour, Xiangxiang Wang, Xiao Feng, and Yongbin Yu, "Attention enhanced network with semantic inspector for medical image report generation," in *2023 IEEE 35th International Conference on Tools with Artificial Intelligence (ICTAI)*, 2023, pp. 242–249.
- [11] Baoyu Jing, Pengtao Xie, and Eric Xing, "On the automatic generation of medical imaging reports," in *Proceedings of the 56th Annual Meeting of the Association for Computational Linguistics*, 2018, vol. 1, pp. 2577–2586.
- [12] Jonathan Giezendanner, Rohit Mukherjee, Matthew Purri, Mitchell Thomas, Max Mauerman, A.K.M. Saiful Islam, and Beth Tellman, "Inferring the past: A combined cnn-lstm deep learning framework to fuse satellites for historical inundation mapping," in *Proceedings of*

- the *IEEE/CVF Conference on Computer Vision and Pattern Recognition (CVPR) Workshops*, June 2023, pp. 2155–2165.
- [13] Oriol Vinyals, Alexander Toshev, Samy Bengio, and Dumitru Erhan, “Show and tell: A neural image caption generator,” in *2015 IEEE Conference on Computer Vision and Pattern Recognition (CVPR)*, 2015, pp. 3156–3164.
 - [14] Hoo-Chang Shin, Kirk Roberts, Le Lu, Dina Demner-Fushman, Jianhua Yao, and Ronald M Summers, “Learning to read chest x-rays: Recurrent neural cascade model for automated image annotation,” in *2016 IEEE Conference on Computer Vision and Pattern Recognition (CVPR)*, 2016, pp. 2497–2506.
 - [15] Ashish Vaswani, Noam Shazeer, Niki Parmar, Jakob Uszkoreit, Llion Jones, Aidan N. Gomez, Lukasz Kaiser, and Illia Polosukhin, “Attention is all you need,” 2017.
 - [16] Alexey Dosovitskiy, Lucas Beyer, Alexander Kolesnikov, Dirk Weissenborn, Xiaohua Zhai, Thomas Unterthiner, Mostafa Dehghani, Matthias Minderer, Georg Heigold, Sylvain Gelly, et al., “An image is worth 16x16 words: Transformers for image recognition at scale,” in *International Conference on Learning Representations (ICLR)*, 2020.
 - [17] Yi Tay, Mostafa Dehghani, Jai Gupta, Dara Bahri, Vamsi Aribandi, Zhen Qin, and Donald Metzler, “Are pre-trained convolutions better than pre-trained transformers?,” 2022.
 - [18] Zhuang Liu, Hanzi Mao, Chao-Yuan Wu, Christoph Feichtenhofer, Trevor Darrell, and Saining Xie, “A convnet for the 2020s,” in *2022 IEEE/CVF Conference on Computer Vision and Pattern Recognition (CVPR)*, 2022, pp. 11966–11976.
 - [19] Cheng Huang, Junhao Shen, Beichen Hu, Mohammad Haqqani, Tsengdar Lee, Karanjit Kooner, Ning Zhang, and Jia Zhang, *Semantic and Visual Attention-Driven Multi-LSTM Network for Automated Clinical Report Generation*, pp. 233–248, 08 2024.
 - [20] John Pavlopoulos, Vasiliki Kougia, and Ion Androutsopoulos, “A survey on biomedical image captioning,” in *Proceedings of the second workshop on shortcomings in vision and language*, 2019, pp. 26–36.
 - [21] Qian Tang, Yongbin Yu, Xiao Feng, and Chenhui Peng, “Semantic and visual enrichment hierarchical network for medical image report generation,” in *2022 Asia Conference on Algorithms, Computing and Machine Learning (CACML)*, 2022, pp. 738–743.
 - [22] Oriol Vinyals, Alexander Toshev, Samy Bengio, and Dumitru Erhan, “Show and tell: A neural image caption generator,” in *2015 IEEE Conference on Computer Vision and Pattern Recognition (CVPR)*, 2015, pp. 3156–3164.
 - [23] Kelvin Xu, Jimmy Ba, Ryan Kiros, Kyunghyun Cho, Aaron Courville, Ruslan Salakhutdinov, Richard Zemel, and Yoshua Bengio, “Show, Attend and Tell: Neural Image Caption Generation with Visual Attention,” Apr. 2016, arXiv:1502.03044 [cs].
 - [24] Jeff Donahue, Lisa Anne Hendricks, Marcus Rohrbach, Subhashini Venugopalan, Sergio Guadarrama, Kate Saenko, and Trevor Darrell, “Long-term Recurrent Convolutional Networks for Visual Recognition and Description,” May 2016, arXiv:1411.4389 [cs].
 - [25] Cheng Huang, Junhao Shen, Qiuyu Luo, Karanjit Kooner, Tsengdar Lee, Yishen Liu, and Jia Zhang, “Latent relationship mining of glaucoma biomarkers: a tri-lstm based deep learning,” *arXiv preprint arXiv:2408.15555*, 2024.
 - [26] Marcella Cornia, Matteo Stefanini, Lorenzo Baraldi, and Rita Cucchiara, “Meshed-Memory Transformer for Image Captioning,” Mar. 2020, arXiv:1912.08226 [cs].
 - [27] Peter Anderson, Xiaodong He, Chris Buehler, Damien Teney, Mark Johnson, Stephen Gould, and Lei Zhang, “Bottom-Up and Top-Down Attention for Image Captioning and Visual Question Answering,” Mar. 2018, arXiv:1707.07998 [cs].
 - [28] Mingjie Li, Rui Liu, Fuyu Wang, Xiaojun Chang, and Xiaodan Liang, “Auxiliary signal-guided knowledge encoder-decoder for medical report generation,” *World Wide Web*, vol. 26, no. 1, pp. 253–270, Jan. 2023.
 - [29] Zhihong Chen, Yan Song, Tsung-Hui Chang, and Xiang Wan, “Generating Radiology Reports via Memory-driven Transformer,” Apr. 2022, arXiv:2010.16056 [cs].
 - [30] Fenglin Liu, Changchang Yin, Xian Wu, Shen Ge, Yuexian Zou, Ping Zhang, Yuexian Zou, and Xu Sun, “Contrastive Attention for Automatic Chest X-ray Report Generation,” Apr. 2023, arXiv:2106.06965 [cs].
 - [31] Yan Yang, Jun Yu, Jian Zhang, Weidong Han, Hanliang Jiang, and Qingming Huang, “Joint embedding of deep visual and semantic features for medical image report generation,” *IEEE Transactions on Multimedia*, vol. 25, pp. 167–178, 2023.
 - [32] Marcella Cornia, Matteo Stefanini, Lorenzo Baraldi, and Rita Cucchiara, “Meshed-memory transformer for image captioning,” in *2020 IEEE/CVF Conference on Computer Vision and Pattern Recognition (CVPR)*, 2020, pp. 10575–10584.
 - [33] Xing Jia, Yun Xiong, Jiawei Zhang, Yao Zhang, Blackley Suzanne, Yangyong Zhu, and Chunlei Tang, “Radiology report generation for rare diseases via few-shot transformer,” in *2021 IEEE International Conference on Bioinformatics and Biomedicine (BIBM)*, 2021, pp. 1347–1352.
 - [34] Zhanyu Wang, Lingqiao Liu, Lei Wang, and Luping Zhou, “R2gengt: Radiology report generation with frozen llms,” *Meta-Radiology*, vol. 1, no. 3, pp. 100033, 2023.
 - [35] Xiao Wang, Yuehang Li, Fuling Wang, Shiao Wang, Chuanfu Li, and Bo Jiang, “R2gensr: Retrieving context samples for large language model based x-ray medical report generation,” *arXiv preprint arXiv:2408.09743*, 2024.
 - [36] Stéphane d’Ascoli, Hugo Touvron, Matthew Leavitt, Ari Morcos, Giulio Biroli, and Levent Sagun, “Convit: Improving vision transformers with soft convolutional inductive biases,” in *Proceedings of the 38th International Conference on Machine Learning (ICML)*, 2021, pp. 2286–2296.
 - [37] Longyu Yang, Hanli Wang, Pengjie Tang, and Qinyu Li, “Captionnet: A tailor-made recurrent neural network for generating image descriptions,” *IEEE Transactions on Multimedia*, vol. 23, pp. 835–845, 2021.
 - [38] Alistair EW Johnson, Tom J Pollard, Nathaniel R Greenbaum, Matthew P Lungren, Chih-ying Deng, Yifan Peng, Zhiyong Lu, Roger G Mark, Seth J Berkowitz, and Steven Horng, “Mimic-cxr-jpg, a large publicly available database of labeled chest radiographs,” *arXiv preprint arXiv:1901.07042*, 2019.
 - [39] Kishore Papineni, Salim Roukos, Todd Ward, and Wei-Jing Zhu, “Bleu: a method for automatic evaluation of machine translation,” in *Proceedings of the 40th annual meeting of the Association for Computational Linguistics*, 2002, pp. 311–318.
 - [40] Chin-Yew Lin and Franz Josef Och, “Automatic evaluation of machine translation quality using longest common subsequence and skip-bigram statistics,” in *Proceedings of the 42nd annual meeting of the association for computational linguistics (ACL-04)*, 2004, pp. 605–612.
 - [41] Ramakrishna Vedantam, C Lawrence Zitnick, and Devi Parikh, “Cider: Consensus-based image description evaluation,” in *Proceedings of the IEEE conference on computer vision and pattern recognition*, 2015, pp. 4566–4575.
 - [42] Jia Deng, Wei Dong, Richard Socher, Li-Jia Li, Kai Li, and Li Fei-Fei, “Imagenet: A large-scale hierarchical image database,” in *2009 IEEE Conference on Computer Vision and Pattern Recognition*, 2009, pp. 248–255.
 - [43] Diederik Kingma and Jimmy Ba, “Adam: A method for stochastic optimization,” in *International Conference on Learning Representations (ICLR)*, San Diego, CA, USA, 2015.
 - [44] Fenglin Liu, Xian Wu, Shen Ge, Wei Fan, and Yuexian Zou, “Exploring and Distilling Posterior and Prior Knowledge for Radiology Report Generation,” in *2021 IEEE/CVF Conference on Computer Vision and Pattern Recognition (CVPR)*, Nashville, TN, USA, 2021, pp. 13748–13757, IEEE.
 - [45] Zhanyu Wang, Hongwei Han, Lei Wang, Xiu Li, and Luping Zhou, “Automated radiographic report generation purely on transformer: A multicriteria supervised approach,” *IEEE Transactions on Medical Imaging*, vol. 41, no. 10, pp. 2803–2813, 2022.
 - [46] Chang Liu, Yuanhe Tian, Weidong Chen, Yan Song, and Yongdong Zhang, “Bootstrapping large language models for radiology report generation,” in *Proceedings of the AAAI Conference on Artificial Intelligence*, 2024, vol. 38, pp. 18635–18643.